Journal of Microbiological Methods 240 (2026) 107343

Contents lists available at ScienceDirect

Journal of Microbiological Methods

journal homepage: www.elsevier.com/locate/jmicmeth

Single-cell RNA seq reveals heterogeneous survival strategies of *Vibrio parahaemolyticus* against ampicillin

Zhangxi Gong [a], Yu Zhou [a,b], Yongbing Ba [e], Yao Yang [a,b], Yingjie Pan [a,b,c],
Yong Zhao [a,b,c,*], Haiquan Liu [a,b,c,d,*]

[a] *College of Food Science and Technology, Shanghai Ocean University, Shanghai 201306, China*
[b] *Shanghai Engineering Research Center of Aquatic-Product Processing & Preservation, Shanghai 201306, China*
[c] *Laboratory of Quality & Safety Risk Assessment for Aquatic Product on Storage and Preservation (Shanghai), Ministry of Agriculture and Rural Affairs, Shanghai 201306, China*
[d] *Engineering Research Center of Food Thermal-processing Technology, Shanghai Ocean University, Shanghai 201306, China*
[e] *Shanghai OE Biotech. Co., Ltd., Shanghai 201212, China*

ARTICLE INFO

Keywords:
scRNA-seq
V. parahaemolyticus
Cellular subpopulations
Drug resistance

ABSTRACT

Bulk RNA-Seq only captures the average gene expression level of bacterial populations and has limitations in analysing functional differences between bacterial subpopulations. Therefore, the study innovatively applied droplet-based single-cell RNA sequencing (scRNA-seq) to resolve ampicillin resistance heterogeneity in *Vibrio parahaemolyticus* (*V. parahaemolyticus*). Findings indicate that high levels of drug resistance (MIC = 1000 μg/mL) demonstrate a significant impact on the phenotypes of interest, particularly when subinhibitory concentrations are considered. To further elucidate the phenotypic heterogeneity results, functionally specialized cellular subpopulations was identified by scRNA-seq, such as an oxidative stress defense subpopulation mediated by *gorA* upregulation, virulence modulation achieved through *exsD*-mediated repression of the type III secretion system, drug resistance conferred by MATE family efflux pumps, protein homeostasis maintained by Hsp20, metabolic reprogramming driven by NirD/YgiW/YdeI family proteins, and membrane damage repair facilitated by *pspA* upregulation. The phenotypic heterogeneity analysis results support some of the newly discovered functional annotations of resistant subpopulations, demonstrating the biological basis of bacterial heterogeneity under antibiotic pressure. The discovery of these functional drug-resistant subpopulations provides deeper insight into *V. parahaemolyticus* resistance and paves the way for developing novel antimicrobial strategies targeting key signaling proteins for population-level coordination.

1. Introduction

Vibrio parahaemolyticus a prevalent food - borne pathogen in marine settings, poses a risk to human health. When people consume raw or inadequately cooked aquatic products tainted with this bacterium, it can result in gastrointestinal disorders (Su and Liu, 2007). *V. parahaemolyticus* exhibits virulence through multiple mechanisms, including adhesins, toxins, and Type III Secretion Systems (T3SS) (Zhang and Orth, 2013). *V. parahaemolyticus* has emerged as a significant pathogen of marine origin. It is the leading cause of foodborne acute gastroenteritis and is increasingly impacting global public health (Velazquez-Roman et al., 2014). China observed a mean annual caseload of 523.5 for confirmed *V. parahaemolyticus* infections over the 11-year period from 2010 through 2020 (Chen et al., 2017; Zheng et al., 2025).

Nowadays, due to the widespread use of antibiotics, the acquisition and spread of antibiotic resistance genes (ARGs) has become widespread (Guo et al., 2025; Lemée et al., 2025). Several studies had shown that *V. parahaemolyticus* is multi-drug resistant (Huan et al., 2018; Jiang et al., 2014; Li et al., 2019; Tan et al., 2022; Xiaofeng et al., 2023). In particular, *V. parahaemolyticus* may enhance resistance by reducing the expression of hydrophilic pore proteins (e.g., OmpF) and decreasing the uptake of β-lactam antibiotics such as ampicillin (Munita Jose and Arias Cesar, 2016; Tan et al., 2022), which is the key focus of our article's exploration.

Next-generation sequencing (NGS) helps to study bacterial drug resistance. A key role of the efflux transporter protein in streptomycin

---

* Corresponding authors at: College of Food Science and Technology, Shanghai Ocean University, Shanghai 201306, China.
E-mail addresses: yzhao@shou.edu.cn (Y. Zhao), hqliu@shou.edu.cn (H. Liu).

https://doi.org/10.1016/j.mimet.2025.107343
Received 12 October 2025; Received in revised form 17 November 2025; Accepted 22 November 2025

resistance had been revealed by transcriptome sequencing (Zhang et al., 2024). Transcriptome analysis of *V. parahaemolyticus* exposed to ampicillin showed that overexpression of nine genes, including genes *VPA0510* and *VPA0252*, enhanced the resistance of *V. parahaemolyticus* to ampicillin (Tan et al., 2022). In Vp2015094, the *luxS* gene associated with the LuxS/AI-2 quorum-sensing system demonstrated significant contributions to both antibiotic tolerance mechanisms and horizontal dissemination of resistance determinants (Jiang et al., 2023).

However, studies of cellular expression heterogeneity at the level of individual bacteria are scarce due to technical limitations. Bulk RNA-Seq reflects the average gene expression of bacterial populations and cannot detect rare cell subpopulations with an abundance of <1 %.In contrast, scRNA-seq can resolve the cellular heterogeneity of complex microbial communities at high resolution, analyze cell types and associated gene expression differences, and identify potential novel therapeutic targets (Wang et al., 2025; Hedlund and Deng, 2018; He et al., 2023). Xu et al. (Xu et al., 2023) reported a technique that can be used to detect transcriptome expression maps of individual bacteria. Ma et al. (Ma et al., 2023) revealed through scRNA-sequencing that heterogeneity within populations is primarily driven by the expression of mobile genetic factors that promote the evolution of antibiotic resistance. The scRNA-seq provided us with a method to explore the drug-resistant heterogeneity of *V. parahaemolyticus* transcriptome map. By studying the adaptations and interactions of individual bacteria, we aim to elucidate the mechanisms underlying bacterial persistence and resistance, identify antibiotic-resistant subpopulations, develop new strategies for the precise diagnosis and treatment of *V. parahaemolyticus* infections, and offer researchers a novel analytical approach.

2. Materials and methods

2.1. Bacterial culture

The experiment utilized *V. parahaemolyticus* strain 49 (hereinafter referred to as VP49), a clinical strain isolated from an acute diarrheal patient at the gastroenterology clinic of Shanghai Hospital, which harbors the virulence gene cluster $tdh^{+}/trh^{+}/tlh^{+}$. The genetic characterization of this bacterium has been comprehensively described in our laboratory's prior study (Li et al., 2017). The cryopreserved strain was thawed and isolated by delineation on Thiosulfate-Citrate-Bile Salts-Sucrose agar plates (TCBS). After incubation at 37 °C for 12–16 h, single colonies exhibiting typical morphological features were selected and inoculated into 10 mL of Tryptic Soy Broth (TSB) supplemented with 3 % NaCl. The culture was then incubated in a shaking incubator at 37 °C and 200 rpm for 10 h to reach the logarithmic growth phase. The bacterial suspension was standardized to a concentration of 10^7–10^8 CFU/mL (OD600nm ≈ 0.5) by turbidimetry, and this standard was verified by the plate - spreading method (the bacterial solution with OD600nm ≈ 0.5 was serially diluted 10^{-6} times, 0.1 mL of the diluted bacterial solution was spread on TCBS, and after 12 h of cultivation, the number of colonies counted was approximately 83–105). Set it aside for later use.

2.2. Dynamic determination of MIC (minimum inhibitory concentration)

The MIC value of ampicillin against VP49 was assessed by micro broth dilution method with reference to CLSI M45-A3 guidelines (Xin et al., 2023).First, the concentration of bacterial suspension was diluted to 10^5 CFU/mL, and a concentration gradient of ampicillin and TSB medium was prepared by double serial dilution, which was added to 96-well microplates at 100 μL per well, and then an equal volume of bacterial suspension was added to make the final concentrations of 8000 μg/mL, 4000 μg/mL, 2000 μg/mL, 1000 μg/mL, 500 μg/mL, 250 μg/mL, 125 μg/mL, 62.5 μg/mL and 31.25 μg/mL, and at the same time, set up a three-replicate experiment and strict quality control (TSB medium negative control and positive control of the drug-free bacterial solution) (Yang et al., 2019).The endpoint was determined by combining visual turbidimetry and quantitative analysis by spectrophotometric method ($OD_{600nm} < 0.1$ was considered as complete inhibition), and the lowest concentration of the drug that completely inhibited the growth of the bacteria was determined as the MIC value.

2.3. Analysis of growth kinetics under different concentrations of ampicillin

Based on the MIC results, six subinhibitory concentration gradients (1000 μg/mL, 500 μg/mL, 250 μg/mL, 125 μg/mL, 62.5 μg/mL, and 31.25 μg/mL) and a blank control group without ampicillin were selected for the determination of growth curves. The activated bacterial suspension was diluted 103-fold in a gradient, mixed with the drug-containing medium in a 100-well honeycomb plate at a ratio of 1:9 (final volume of 200 μL per well), and the OD values were recorded by a Bioscreen C automated growth curve analyser at 37 °C, 600 nm wavelength. According to CLSI guideline M07-A10, we conducted three independent experimental runs for every concentration level using freshly aliquoted reagents each time. Subsequently, the modified Gompertz model was used to fit the data and extract the key parameters, which were analysed by Origin 2024 software to obtain the parameters of the maximum specific growth rate ($\mu_{\max}$) and the Lag Time (LT) (the model's superiority was verified by $R^2 > 0.98$ and residual analysis). The specific formula is as follows:

$$y = A + B^{*}exp\left\{ -\exp\left[\frac{\mu_{\max}(C - x)}{A} + 1 \right] \right\}$$

A represents the initial inoculum size (CFU/mL); B represents the difference between the maximum bacterial concentration and the initial bacterial concentration (CFU/mL); C represents LT (h); x represents time (h); y represents the total number of bacteria at that time point (CFU/mL).

2.4. Measurement of swimming and swimming ability

To quantify the dose-effect relationship between colony extension diameter and drug concentration, a differential agar concentration model (swimming: LB plates containing 0.3 % agar; swarming: LB plates containing 1 % agar) was designed with modifications based on the description by Song et al. (Song et al., 2025)Ampicillin was added to the LB agar medium after cooling to 40–50 °C post-sterilization to prevent thermal degradation. 5 μL of the bacterial suspension with adjusted OD_{600nm} to 0.5 was aseptically spotted in the center of the swimming and swarming plates. After 12 and 24 h of incubation at 37 °C, the diameter of the colony expansion zone was measured to assess the inhibitory effect of ampicillin on bacterial motility.

2.5. Determination of the dynamic formation capacity of biofilm

Crystal violet staining was employed to quantitatively analyze the ability of biofilm formation (Zhu et al., 2025). The activated bacterial suspension and drug-containing TSB medium were added into 24-well polystyrene plates at a ratio of 1:99 (*v*/v). The mixture was gently mixed and then incubated at 37 °C under static conditions to promote biofilm maturation prior to staining. Following 72 h of continuous culture, the bacterial solution in each well was discarded and washed with 0.01 M PBS for three times to remove the bacteria in the free stat. After drying at 60 °C for 30 min, add 1 mL of 0.1 % crystal violet staining solution for 20–30 min, discard the staining solution and wash with 0.01 M PBS for 3 times to remove the residual dye, add 1 mL of 95 % ethanol solution and vortex mixing to fully dissolve the biofilm bound to the bottom of the wells, and then suck 200 μL of the solution for 20 min and then transfer it to a 96-well plate, and then measure the OD value by a microplate reader at 600 nm.

2.6. Cell membrane damage assay

The Bacterial Viability/Toxicity Assay Kit employs a dual-fluorescence staining strategy to evaluate membrane integrity, utilizing two fluorophores: the global nucleic acid dye NucGreen stains live and dead bacteria green; the membrane-breakage-specific labelling dye EthD-III stains only dead bacteria with damaged cell membranes red. Mix NucGreen, EthD-III and 0.85 % NaCl solution in the ratio of 1:2:8 to obtain 100× working solution.

Transfer 1 mL of the activated bacterial suspension into a 1.5 mL centrifuge tube and centrifuge at 5000 rpm for 15 min at 4 °C, then discard the supernatant. The precipitate was resuspended in 1 mL of 0.01 M PBS and centrifuged again at 5000 rpm for 15 min, and the procedure was repeated twice to ensure complete removal of extracellular metabolites. Add 1 μL of working solution to 1 mL of bacterial suspension and mix thoroughly, incubate at room temperature and protected from light for 15 min. Subsequently, 10 μL of the stained bacterial suspension was placed on a glass microscope slide with an 18 × 18 mm coverslip. Imaging was carried out with the use of a confocal laser scanning microscope. (CLSM; TCS SP8, Leica Microsystems) with a 20× objective lens. Excitation/emission wavelengths were configured at 488 nm/510–610 nm and 552 nm/571–630 nm to detect viable and nonviable cells, respectively (Yu et al., 2023).

2.7. Cytotoxicity test

The cytotoxicity of ampicillin against VP49 was evaluated using the CCK-8 assay (Zeng et al., 2024). The activated bacterial suspension was incubated at 37 °C for 12 h, 24 h, 36 h and 72 h according to the dosing regimen of the growth curve assay described previously. The bacterial suspension was centrifuged at 5000 rpm for 15 min to collect the cells, and then resuspended in PBS, and washed 2–3 times through repeated centrifugation-resuspension cycles. Following addition of 10 μL CCK-8 reagent per well, the plate was incubated for 2 h under light-protected conditions prior to absorbance measurement at 450 nm using a microplate reader.

2.8. Drug sensitivity testing

VP49 at a concentration of approximately 1×10^8 CFU/mL was spread evenly on LB medium. Sterile tweezers were used to aseptically place antimicrobial susceptibility discs onto the inoculated agar surface. The plates were incubated at 37 °C for 24 h in a humidified incubator. Following this, the inhibition zones were carefully measured using a digital caliper to assess the antimicrobial activity.

2.9. Permeabilization

Bacterial cells were collected via centrifugation at 4 °C. The supernatant was removed and cell pellets were resuspended in 2 mL of prechilled 4 % formaldehyde (Sigma, 47608). After overnight incubation with shaking at 4 °C, the cells were centrifuged at 4000 rpm for 5 min at 4 °C to remove the fixative, and then washed twice with 1 mL of PBS-TRI (1 × PBS, supplemented with 0.1 % Tween-20 and 0.1 U/mL mouse RNase inhibitor (Vazyme, R301)). The supernatant was removed and cells were resuspended in 200 μL PBS-TRI (1 × PBS supplemented with 0.1 % Tween-20 and 0.2 U/mL Murine RNase inhibitor (Vazyme, R301)).

2.10. Library construction and sequencing

A protocol provided by the VITAPilote® kit (M20 Genomics, R20114124) was followed to prepare the bacterial single-cell RNA-Seq library. Following cell wall digestion, in situ reverse transcription of fixed bacterial cells was conducted using random primers. The VITACruiser® Single Cell Partitioning System (M20 Genomics, Hangzhou, China) was utilized to carry out droplet barcoding for a single bacteria. Bacteria, DNA extension reaction mix, and hydrogel barcoded beads were encapsulated using the VITACruiser. The aqueous phase containing cDNAs was purified using magnetic beads. The cDNAs were then amplified by PCR and subjected to a second round of purification with magnetic beads. All resulting products were combined to create a standard sequencing library. Finally, the library was sequenced on the NovaSeq 6000 platform using the S4 Reagent Kit with 150-bp paired-end reads.

2.11. scRNA-seq data processing

For scRNA-seq data, FASTQ files were processed using the VITAseer v1.2 (M20 Genomics Company). The raw sequencing reads were processed with Cutadapt (v3.7) for quality trimming. Read1 was parsed to extract UMIs and cell-specific barcodes, which were merged if they matched a reference barcode with ≤1 Hamming distance. Read2 was aligned to the target genome using STAR (v2.7.10a, default settings), retaining only uniquely mapped reads. For single-cell analysis, we employed Seurat (v4.3.0.1) with modified parameters where specified. Cells expressing <100 genes and genes detected in <5 cells were excluded. Data were log-normalized (NormalizeData), and the top 2000 variable genes were selected (FindVariableFeatures) and scaled (ScaleData). Dimensionality reduction was performed via PCA (50 PCs), followed by UMAP visualization and Louvain clustering (FindClusters, resolution 0.5–1.5). Cluster robustness was confirmed across resolutions. Differential gene expression (DEG) was assessed using FindMarkers (logFC threshold = 0.25).

2.12. Statistical methods

All experimental procedures were conducted with three independent biological replicates. The *p*-value was calculated using a two-tailed Student's *t*-test. Statistical significance was established at the 95 % confidence level (p-value <0.05). Data visualization and graphical representations were generated using OE Cloud Platform (cloud.oebiotech.com).

3. Result

3.1. MIC and growth heterogeneity

Drug sensitivity testing revealed that the MIC of ampicillin against strain VP49 was 1000 μg/mL, which was significantly higher than the threshold of CLSI Vibrio tolerance standard (≥32 μg/mL), suggesting that the strain has formed a strong resistance phenotype to ampicillin. Combined with related literature data, it was hypothesised that it might be associated with carrying homologous resistance genes, such as the novel β-lactamase gene *blaV110* or similar enzymatic machines (Chiou et al., 2015). In order to further resolve the dose-dependent effects of ampicillin on bacterial growth kinetics, growth curves were next measured and plotted, which can visualise the specific effect of ampicillin on VP49 growth at MIC and subinhibitory concentrations.

The ampicillin's effect on the bacteria is closely related to the concentration gradient (Fig. 1A-B). Under a certain concentration, bacterial growth was nearly completely inhibited, and the maximum growth rate was significantly reduced compared to the control group. Under a lower ampicillin concentration, although the bacteria could still proliferate slowly, the maximum growth rate was significantly lower than that in the control group ($p < 0.05$), with a reduction amplitude of 47.4 %. In addition, the survival time in the subinhibitory concentration group showed a linear increase ($R^2 = 0.982$), reaching 12.3 ± 0.5 h at the lower ampicillin concentration, which was significantly higher than 6.8 ± 0.3 h in the control group ($p < 0.01$).

The data in Fig. 1B show that, although the lower antibiotic concentration allows slow bacterial proliferation, its maximum growth rate

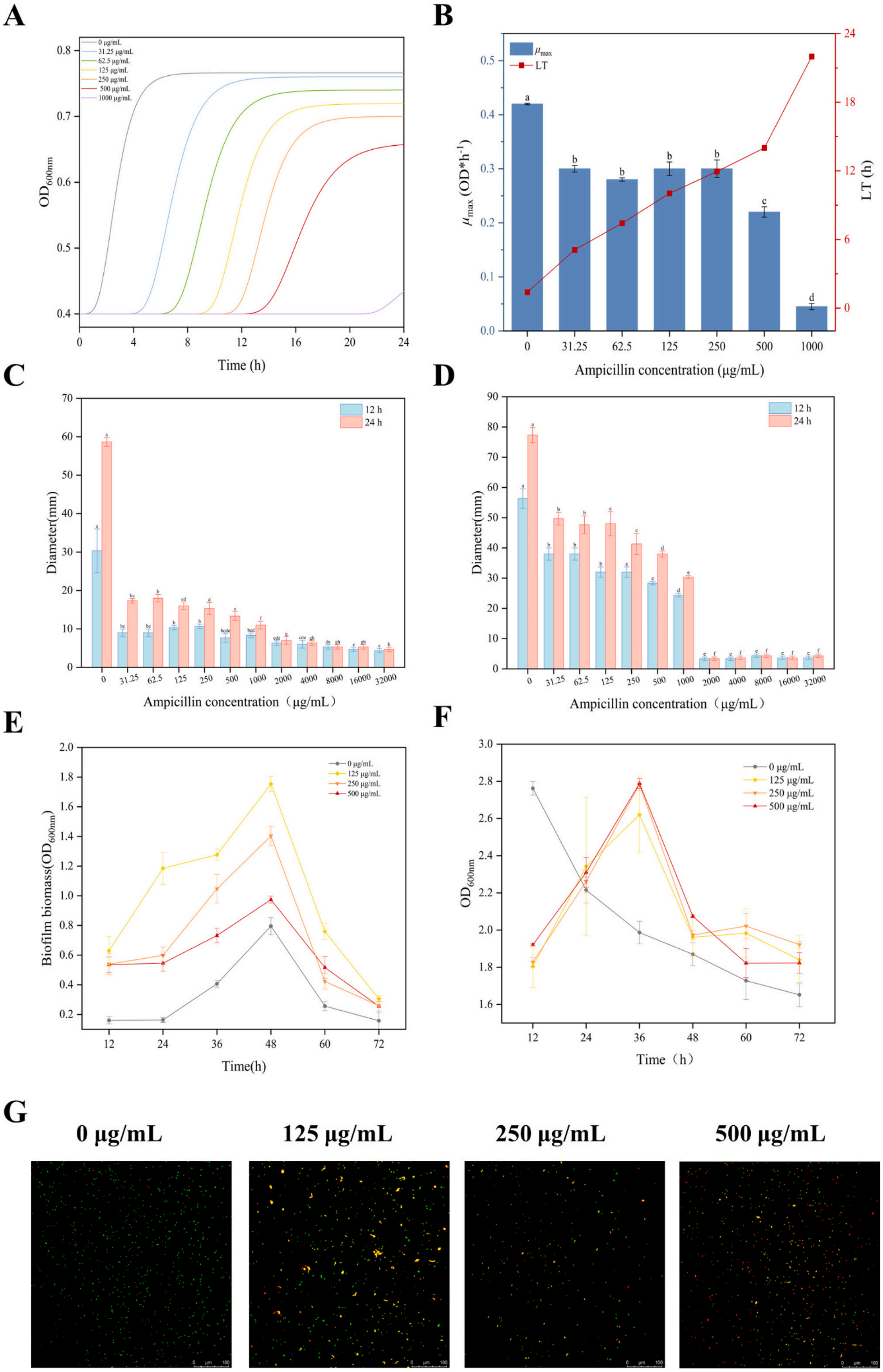

Fig. 1. (A) Growth curves of VP49 at 1000 μg/mL, 500 μg/mL, 250 μg/mL, 125 μg/mL, 62.5 μg/mL, 31.25 μg/mL and 0 μg/mL ampicillin, respectively. (B) Fitting of the LT and μ_{max} based on the Gompertz model. Data are presented as mean ± SD ($n = 3$), different letters indicate $p < 0.05$ intergroup differences, one-way ANOVA. (C and D) Swimming and surging ability of VP49 in a sub-MIC concentration environment. Data are presented as mean ± SD (n = 3), different letters indicate $p < 0.05$ intergroup differences, one-way ANOVA. (E) Quantification of VP49 bioepithelial membrane formation capacity by crystal violet staining in a sub-MIC concentration environment. (F) Cellular activity of VP49 by CCK-8 assay in a sub-MIC concentration environment. (G) Confocal laser microscopy (CLSM) observation of membrane integrity of NucGreen/EthD-III double staining (20× objective, scale bar = 100 μm). Different lowercase letters (a, b, c…) indicate significant differences between groups ($p < 0.05$, using the ANOVA test); the same letters indicate no statistically significant differences.

is still significantly lower than that of the control group. In addition, the survival time increases linearly with the ampicillin concentration, indicating that the subinhibitory concentration can delay bacterial growth and force the bacteria to take a longer time to activate the stress response mechanism to adapt to the ampicillin stress environment.

When the concentration is close to the lower threshold, the maximum growth rate drops to 0.22 OD * h^{-1}, which is significantly different from 0.41992 OD * h^{-1} in the control group ($p < 0.05$). Considering that this concentration not only significantly reduces the maximum growth rate of bacteria but also has sufficient clinical relevance, it was selected as the reference threshold for subsequent experiments.

3.2. Swimming and swarmming ability of VP49 in different concentrations of ampicillin cellular subpopulations

In this study, the effect of ampicillin treatment on the swimming and swarming ability of VP49 was investigated using the soft LB agar assays. The inhibitory effect of ampicillin on the swimming and swarming ability of VP49 at sub-MIC concentration showed concentration-dependent and time-dynamic recovery (Fig. 1C-D). With the increase of drug concentration, the swimming ability decreased in a gradient, and at 1/4 MIC (250 μg/mL), the swimming ability was significantly weakened, while at the same concentration, the inhibition of swarming ability was more obvious; it is noteworthy that both motilities demonstrated partial restoration at 24 h; at near 1/2 MIC (500 μg/mL), the recovery extents of the two motilities became comparable. The complete inhibition of both motilities at MIC concentration corroborated the reduced $\mu_{\max}$ and prolonged LT observed in growth curves, suggesting that this concentration may compel bacteria to abandon energy-intensive motility strategies in favor of survival prioritization to partially mitigate drug stress. The differential recovery patterns likely originate from distinct physiological dependencies: swimming ability is highly dependent on flagellar anchoring and the integrity of the peptidoglycan layer, which ampicillin impairs by directly disrupting cell wall synthesis, whereas limited metabolic adjustments (e.g., flagellin repair) at low concentrations may transiently restore some motility functions; in contrast, recovery of swarming ability is more reliant on quorum sensing - mediated coordination, such as the activation of the community sensing system promotes the secretion of signaling molecules or extracellular matrices, thereby increasing the efficiency of co-migration between bacteria.

3.3. Biofilm biomass formation capacity of VP49 at subinhibitory concentrations

As depicted in Fig. 1E, strain VP49 demonstrated a unique biphasic dose-response of biofilm formation at subinhibitory concentrations of ampicillin. Biofilm formation was minimum level under pure culture conditions without antibiotics, representing the basal level. Upon introduction of subinhibitory concentrations of penicillin, biofilm formation was significantly enhanced and peaked at a concentration of 125 μg/mL, suggesting that this concentration provided the optimal stimulus intensity to induce a maximal stress response. However, as the penicillin concentration rose further, biofilm formation showed a decreasing trend, which may be due to the fact that the higher intensity of antibiotic stress began to produce a more significant inhibition of the overall metabolic activity and proliferation rate of the bacteria, limiting the synthesis of energy and substances for biofilm construction or leading to a decrease in the viability of some of the cells. Despite this inhibitory effect at high concentrations, a key finding was that the experimental groups containing penicillin all had significantly higher biofilm formation than the antibiotic-free control group. This provides strong evidence that the presence of penicillin itself constitutes a sustained and potent inducer of biofilm formation throughout the range of subinhibitory concentrations tested, inducing a basal level of stress sufficient to overcome baseline inertia under pure culture.

3.4. Cell viability of VP49 at subinhibitory concentrations

From Fig. 1F, it was found that the inhibitory effect of ampicillin on the activity of VP49 was related to the time and concentration: the concentration of 125–500 μg/mL of ampicillin could significantly inhibit the activity of the bacteria in 12–36 h, and there was no significant difference in the inhibitory effect of ampicillin on the bacteria in different concentrations in this range; the growth trend of 125 and 250 μg/mL groups tended to be the same as that of the control group after 36 h, which indicated the inhibitory effect, whereas the high concentration of 500 μg/mL showed an additional inhibitory effect on cellular activity at around 49 h, resulting in a significant decrease in the number of surviving bacteria.

3.5. Cell membrane damage of VP49 in subinhibitory concentrations

The effect of ampicillin on VP49 at subinhibitory concentrations was assessed by monitoring color changes using CLSM. Analysis of Fig. 1G revealed that a low concentration (125 μg/mL) induced partial membrane permeability alterations, pushing cells into a sublethal state. This was evidenced by a significant increase in yellow-fluorescing organisms overlaid on red and green signals ($p < 0.01$), indicating that NucGreen penetrated live and partially dead cells with compromised membranes. Concurrently, EthD-III-labeled red fluorescence suggested progressive membrane damage. As ampicillin concentrations rose, the proportion of yellow organisms declined sharply, while red fluorescence intensified ($p < 0.001$), reflecting a transition from “partially damaged” to “fully ruptured” membranes. The control group (0 μg/mL) exhibited minimal red fluorescence, attributable to natural bacterial death or procedural artifacts. The significantly higher dead-to-live ratio in treated groups confirmed that ampicillin not experimental manipulation directly caused membrane damage and cell death.

These findings imply that subinhibitory antibiotics may pose ecological risks by facilitating resistance gene transfer or enhancing virulence. Future work should integrate scRNA-seq to dissect heterogeneous regulatory networks in sublethal populations and identify membrane repair targets, enabling a comprehensive evaluation of ampicillin’s ecological impact and therapeutic potential.

3.6. Sequencing data processing, filtering, and gene annotation

The lack of an inhibition zone around the drug-sensitive tablets indicated that VP49 was resistant to ampicillin (Fig. 2A). It cultures were mixed thoroughly after individual culturing (Fig. 2B) and subsequently prepared for scRNA-seq (Fig. 2C). The raw sequencing data were filtered, and the effective droplet metrics plot demonstrated that the unique molecular identifier (UMI) of cells positively correlates with changes in the number of expressed genes (Fig. 2D-E). The sequencing results of the retained cells underwent quality control before (Fig. 2F) and after filtering (Fig. 2G). Genes not expressed in all cells were removed, cells with fewer than 10 expressed genes were filtered out, and cells meeting these criteria were classified as high-quality cells for subsequent analysis.

3.7. scRNA-seq revealed different cellular subpopulationss under ampicillin stress

Sequencing high-quality cells generates ultra-high dimensional data with tens of thousands of rows and columns representing cells and genes. Highly variable genes within the cellular subpopulations are selected to derive new dimensions from the tens of thousands of genes, thereby maximizing the information retained from the sample data. Unsupervised dimensionality reduction clustering was applied to the cell sequencing results, yielding 18 distinct cell clusters (Fig. 3A). VP49 was

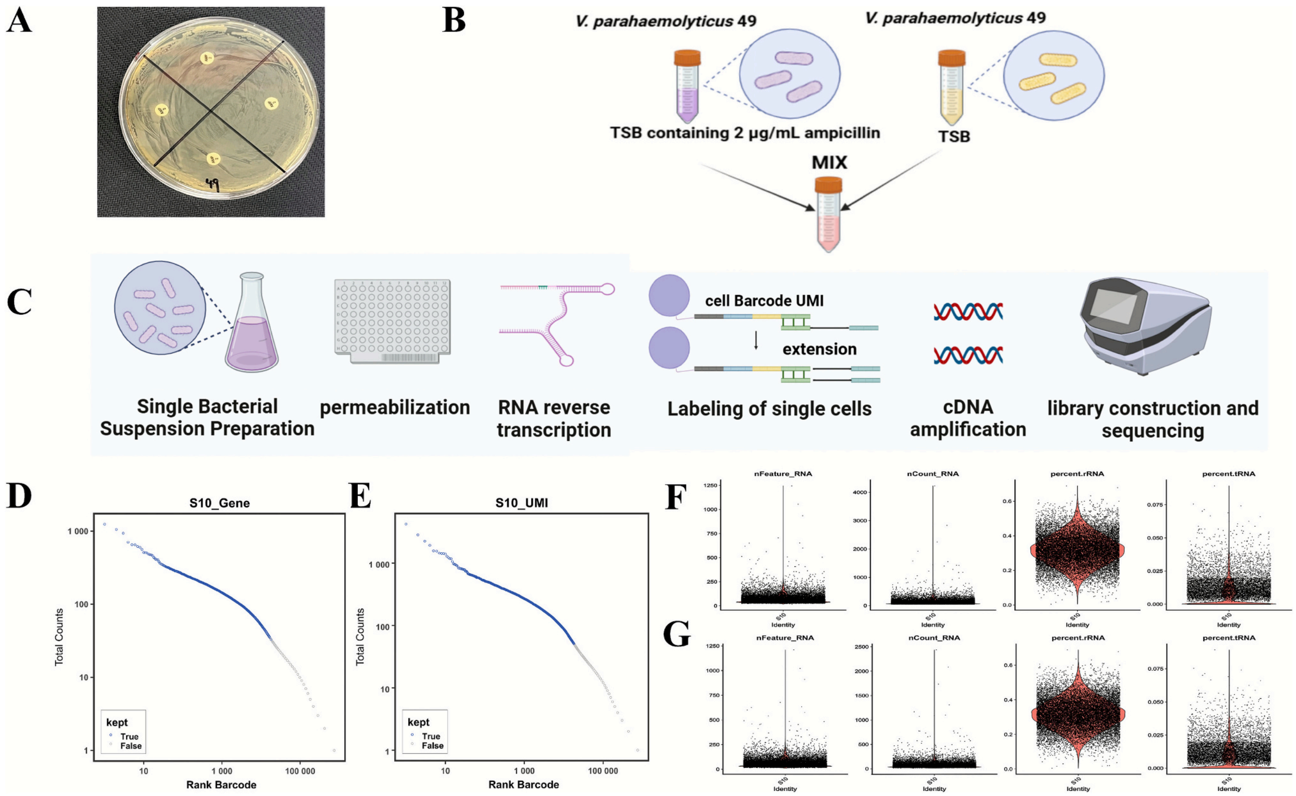

Fig. 2. (A) Results of a drug-sensitive tablet assay of ampicillin at 2 μg/mL. (B) Bacterial culture procedure. (C) M20 Microbial scRNA-seq procedure. (D and E) Plots of effective droplet indexes in each sample, with the horizontal coordinates indicating the cell number sequence (sorted from low to high according to the number of UMIs or genes contained in the cells), and the vertical coordinates indicating the corresponding number of UMIs and genes in the cells. The blue dots indicate cells retained in STARsolo after filtering according to the EmptyDrops_CR algorithm, and the gray ones are cells filtered out in STARsolo. (F and G) Violin plots of each QC metric before and after filtering low-quality cells. (For interpretation of the references to color in this figure legend, the reader is referred to the web version of this article.)

subjected to various treatments, resulting in differential gene expression levels. Thousands of cells were classified into subpopulations using a reduced-dimensional clustering method, revealing heterogeneity in gene expression patterns among the different subpopulations.

Cell counts were performed for 18 cell Clusters under unsupervised dimensionality reduction Clustering (Fig. 3B). After STAR quality control filtering and the removal of cells with abnormal or low gene expression, 18,279 cells remained. Cluster 1 contained 8977 cells, significantly more than any other subpopulation. Correlation analysis between different cellular subpopulationss revealed that the correlation scores between subpopulations and the main population were relatively low (max = 0.61) (Fig. 3C), indicating heterogeneity among subpopulations.

Each cellular subpopulations possesses specific marker genes. A marker gene is highly expressed in most cells of a given population and only in a small fraction of the remaining population, showing significant up regulation compared to other populations. Marker genes help determine the functional type of cells. Cell cluster functions can be defined based on the gene annotations and functional annotations of marker genes. The heatmap of marker genes (Fig. 3D) suggested that the high expression of these genes may explain the distinct gene expression patterns of VP49 under antibiotic treatment.

3.8. *scRNA-seq revealed different expression patterns of cellular subpopulations under ampicillin culture*

3.8.1. *Cells in Cluster 2 expressed strong oxidative stress*

The product of *gorA* (*VP-RS00355*) is glutathione disulfide reductase (GSR), identified in the GO database as having functions related to “cellular response to oxidative stress” and “cellular redox homeostasis” (Table 1). Glutathione is a key component of the cellular antioxidant defense system and plays a crucial role in the maintenance of cellular integrity by scavenging free radical (Ghezzi, 2005). This is typically associated with bacterial protein oxidation and the resultant aggregation, leading to significant cytotoxicity. A homologue of glutathione reductase, AbGSR, has been shown to play a significant role in antioxidant-mediated host defense mechanisms (Herath et al., 2017). Ji et al. demonstrated that glutathione reductase from *C. psychrerythraea* could complement an *E. coli* glutathione reductase deletion strain in oxidative stress growth assays, highlighting its potential utility as an antioxidant enzyme in heterologous systems (Ji et al., 2015).

The high expression level of *gorA* (*VP-RS00355*) in Cluster 2 may indicate intense oxidative stress in the cell as a response to antibiotic treatment (Fig. 4A). Enrichment analysis of other marker genes in Cluster 2 revealed significant enrichment in pathways related to “cellular responses to oxidative stress”, “cell wall organization”, “cellular response to nutrient levels”, “and cellular response to starvation” (Fig. 4B). This observation suggests that bacterial oxidative stress triggers the activation of antioxidant defense systems to mitigate antibiotic-induced metabolic dysregulation linked to cell death. Elevated *gorA* expression enhances bacterial survival under stress by maintaining redox homeostasis, thereby promoting persistence and host colonization (Belenky et al., 2015; Upadhyay and Fu, 2013).

3.8.2. *Cells in Cluster 4 revealed differences in virulence*

VP-RS08180 in Cluster 4 encoded the T3SS regulon anti-activator ExsD (Table 1). The T3SS is a key virulence factor in *V. parahaemolyticus* (Anggramukti et al., *2024*; Plaza et al., *2024*; Tanabe et al., *2024*). Studies have shown that ExsD can inhibit the T3SS in *Pseudomonas aeruginosa* (Brutinel et al., *2010*; Urbanowski et al., *2005*).

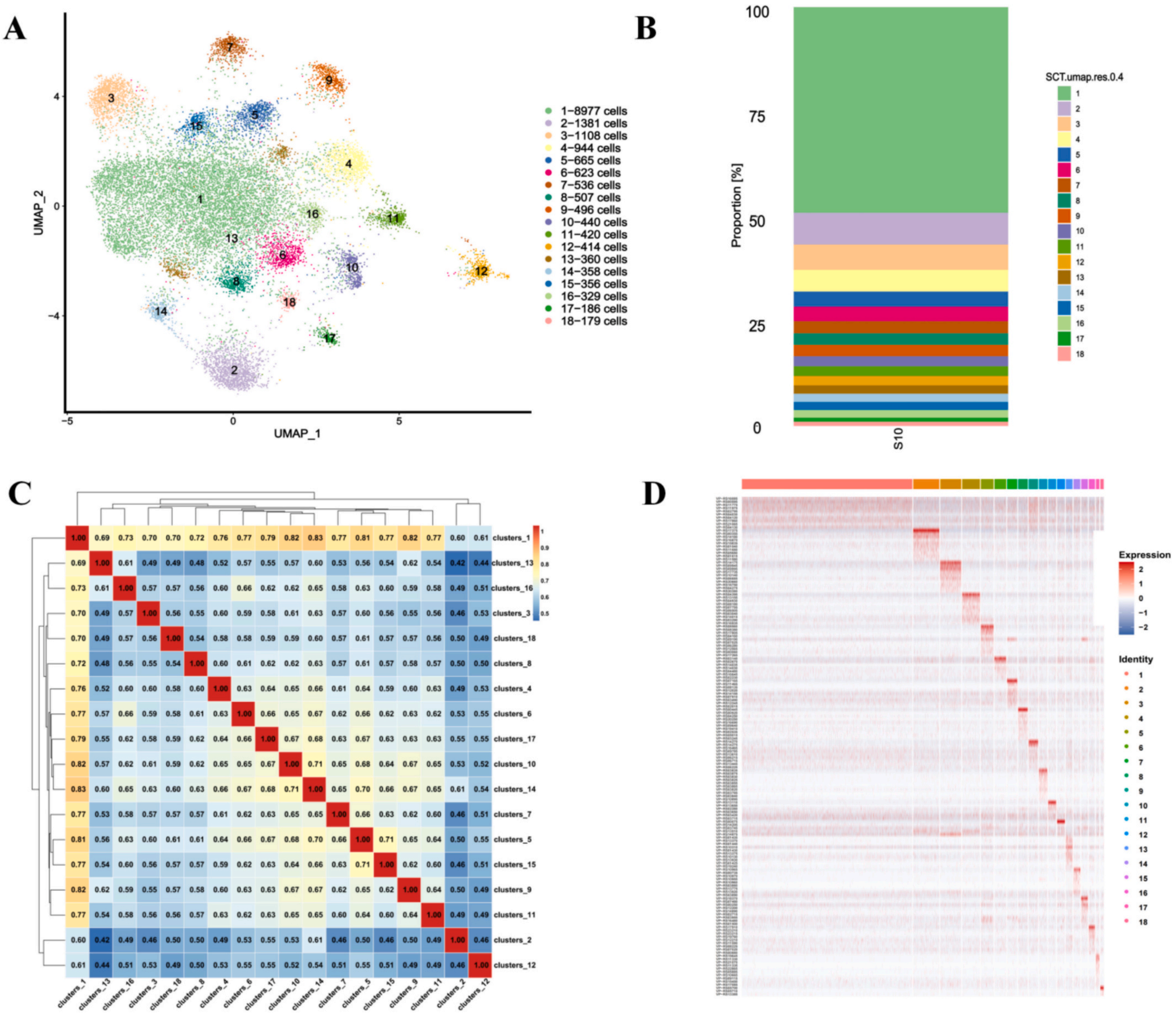

Fig. 3. (A) Downscaling and Clustering plot of gene expression levels, the horizontal and vertical coordinates represent the first and second principal components of downscaling, respectively, and each point in the plot represents a cell, with different Clusters of cells distinguished by different colors. (B) Proportion plot of the number of cells contained in different cell Clusters. (C) Heatmap of correlation analysis of 18 Clusters, the horizontal and vertical coordinates represent different Clusters, the value represents the correlation size, the higher the value, the higher the correlation, the redder the color, the stronger the correlation. (D) Heatmap of top10 marker gene expression, horizontal coordinates are cell Clusters, vertical coordinates are marker genes, yellow color in the graph indicates high expression and purple color indicates low expression. (For interpretation of the references to color in this figure legend, the reader is referred to the web version of this article.)

While the T3SS regulates lateral flagellar assembly genes and swarming motility via the PhoR signaling hub (Zhang et al., 2020). ExsD in *V. parahaemolyticus* functions as a homologue of the *P. aeruginosa* counterpart (Zhou et al., 2010).

VP-RS08180 in Cluster 4 was performed for high gene expression (Fig. 4C). Detailed gene annotation in the Virulence Factor Database (VFDB) provided insights into virulence-related functions. The marker genes of Cluster 4 were compared with the VFDB, revealing significant annotations such as "*pdhB*-Adherence", "MAM7-Adherence," "two-component sensor PprA-Adherence," "Hemolysin A," and "*hemL*-Heme biosynthesis" (Fig. 4D).

Cells in Cluster 4 exhibited significant expression of virulence-related genes under antibiotic treatment. However, ExsD, which inhibited the T3SS of *V. parahaemolyticus*, demonstrated the most significant difference (*VP-RS08180* showed the largest fold change in gene expression in Cluster 4.). This suggested that the T3SS may not be the preferred mechanism for VP49 to express virulence under unfavorable conditions.

3.8.3. Cells in Cluster 7 exhibited a response to antibiotics

VP-RS07165 is identified as a MATE family efflux transporter, involved in antibiotic response as noted in the GO database (Table. 1). The Multidrug and Toxic Compound Extrusion (MATE) family is one of five key multidrug efflux transporter protein families (Kuroda and Tsuchiya, 2009). MATE family integral membrane proteins contribute to multidrug resistance by exporting a variety of therapeutic drugs across cell membranes (Lu, 2016).

VP-RS07165 showed high expression in Cluster 7 (Fig. 4E). Enrichment analysis of other marker genes in Cluster 7 revealed significant enrichment in functional categories such as "AMP binding" and "response to antibiotics" (Fig. 4F). These findings suggested that a subset of cellular subpopulationss in VP49 exhibited highly sensitive gene

Table 1
marker genes and functions of different clusters, p_val_adj represents the significance of the gene change, less than 0.05 is considered significant.

Marker gene	Cluster	gene_description	GO_term	p_val_adj
VP-RS00355	2	glutathione-disulfide reductase	cellular response to oxidative stress，cell redox homeostasis	0
VP-RS08180	4	T3SS regulon anti-activator ExsD		2.8×10^{-246}
VP-RS07165	7	MATE family efflux transporter	response to antibiotic	0
VP-RS00075	12	Hsp20 family protein	protein stabilization	0
VP-RS19645	17	NirD/YgiW/YdeI family stress tolerance protein	periplasmic space	0
VP-RS05700	18	phage shock protein PspA	plasma membrane	0

expression in response to antibiotic stress.

3.8.4. Cells in Cluster 12 expressed heat shock proteins

VP-RS00075 is categorized as a heat shock protein 20 (hsp20) family protein, involved in maintaining protein stability, according to the GO database (Table 1). Qi et al. demonstrated that heterologous expression of the hsp20 gene from *Oenococcus oeni* significantly improved the resistance of the host *E. coli* bacteria against stress conditions (Qi et al., 2020). Bhowmick et al. found that hsp20 played a crucial role in most stress conditions (Bhowmick et al., 2023). Yusof et al. found that GaSGT1, a homologue of hsp20, enhanced cellular heat resistance and acted as a molecular chaperone in response to temperature stress (Yusof et al., 2016).

VP-RS00075 was highly expressed in Cluster 12 (Fig. 4G). Enrichment analysis of marker genes in Cluster 12 revealed significant enrichment in functional categories related to “response to heat” and “protein stabilization” (Fig. 4H). These results suggested that Cluster 12 may help maintain cellular stability by secreting heat shock proteins in response to antibiotic treatment.

3.8.5. Cells in Cluster 17 expressed a protein controlling bacterial stress-induced responses

VP-RS19645 in Cluster 17 is a NirD/YgiW/YdeI family stress tolerance protein that controls bacterial stress-induced responses (Table. 1). Pranjal et al. found that genes responsible for stress tolerance proteins (NirD/YgiW/YdeI) in the bacteria were up regulated during Sono-Fenton process (Pranjal et al., 2023). It has been found that NirD curbs the response coordinated by the signaling molecules guanosine tetraguanosine and guanosine pentaphosphate by inhibiting the activity of RelA in *Escherichia coli*, enabling the bacteria to adapt to environmentally stressful conditions by regulating their metabolism (Léger et al., 2021). A study had identified YgiW in *Escherichia coli* as a stress protein by using the pollutant cis-dichloroethylene (Lee et al., 2010). Arunima et al. identified YdeI as an important protein that regulates *S. enteritidis* virulence and adaptation to stress during infection (Arunima et al., 2020).

The high expression of *VP-RS19645* in Cluster 17 (Fig. 3I). Enrichment analysis of other marker genes for Cluster 17 showed that multiple functional categories related to peptide metabolism, enzyme activity, biosynthetic pathways, were significantly enriched (Fig. 4J). The above results indicated that the growth and metabolism of cells in Cluster 17 were affected when the cells were in an environment containing antibiotics.

3.8.6. Cells in Cluster 18 expressed the phage shock protein PspA

VP-RS05700 (*pspA*) encodes the phage shock protein PspA, which is involved in cytoplasmic membrane formation, as indicated in the GO database (Table 1). PspA is the key effector of the phage shock protein (Psp) system, maintaining the integrity and function of the bacterial inner membrane (Junglas et al., 2021). Standar et al. reported that PspA in *E. coli* stabilized the cytoplasmic membrane under stress conditions (Standar et al., 2008). The *pspA* gene was strongly induced under conditions that disrupt membrane integrity (Vrancken et al., 2008). Cui et al. discovered that the absence of PspA protein impairs the recovery of *Salmonella typhimurium* from thermal injury (Cui et al., 2018).

High *pspA* expression in Cluster 18 (Fig. 4K) was significantly enriched in the “plasma membrane” functional category (Fig. 4L). Under antibiotic treatment, VP49 may have differentiated a population of cells involved in the plasma membrane response through high expression of the PspA protein.

4. Conclusion

The study deciphers the resilience mechanisms of VP49 in ampicillin-compromised environments through scRNA-seq. By integrating scRNA-seq with phenotypic analyses, we demonstrate that bacterial survival under subinhibitory antibiotic pressure is orchestrated by specialized cellular consortia rather than uniform adaptation. Crucially, key phenotypic heterogeneity changes find an explanation here: the significant motility suppression aligns with *exsD* mediated repression of the T3SS in a dedicated subpopulation, indicating strategic resource reallocation under stress. Conversely, the biphasic biofilm induction corresponds to *pspA* expressing subpopulations executing membrane damage repair—a critical adaptation for surface colonization relevant to both clinical and environmental persistence. Beyond these explicit phenotype-transcriptome linkages, we uncovered latent survival modules with therapeutic implications. The *gorA* driven oxidative defense subpopulation and NirD/YgiW/YdeI-mediated metabolic reprogrammers represent novel antibiotic tolerance nodes, while MATE efflux specialists mechanistically explain the strain’s exceptional MIC phenotype. These functionally partitioned subpopulations collectively establish an interdependent resistance network, where detoxification, structural maintenance, and metabolic flexibility are distributed across cellular task forces. This paradigm carries significant implications for antibiotic applications. In clinical settings, such heterogeneity may drive treatment failure by enabling subpopulation-mediated survival rebound. In environmental contexts (e.g., aquaculture systems), residual subinhibitory antibiotics could amplify this heterogeneity, selecting for pre-adapted consortia. The *exsD* attenuated virulence state further suggests potential pathogenicity modulation during antibiotic exposure. Our findings nominate actionable targets within this adaptive network: Efflux specialists and membrane protectors emerge as priority candidates for adjuvant development. By mapping single-cell strategies to population survival, this work provides a roadmap for disrupting cooperative resistance—informing next-generation antimicrobials designed to dismantle bacterial collective resilience in both therapeutic and environmental reservoirs.

5. Discussion

The exceptional ampicillin resistance (MIC = 1000 μg/mL) observed in VP49 aligns with the global trend of rising β-lactam resistance in vibrios, as evidenced by high resistance rates in Shanghai aquatic products (Xiao et al., 2023; Yu et al., 2016). This resistance correlates with the accumulation of antimicrobial resistance genes (ARGs) driven by mobile genetic elements (Fang et al., 2023). For instance, the significant inhibition of swarming motility (Fig. 1C-D) directly aligns with *exsD*-mediated repression of the T3SS in Cluster 4, indicating strategic resource reallocation under antibiotic stress. Similarly, the peak biofilm formation at subinhibitory concentrations (125 μg/mL; Fig. 1E)

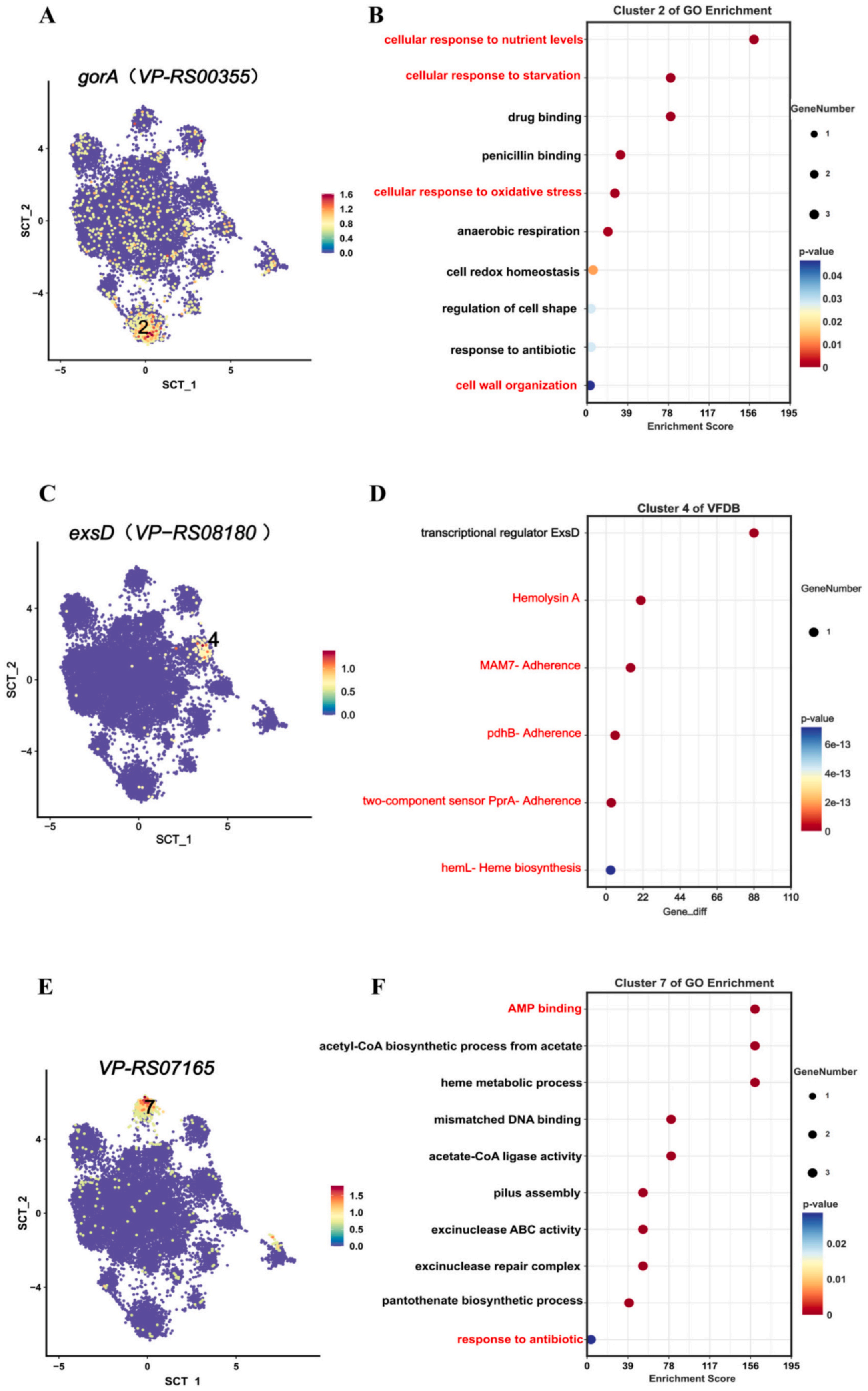

Fig. 4. Featureplots of the marker gene of Cluster 2 (A), Cluster 4 (C), Cluster 7(E), Cluster 12 (G), Cluster 17 (I), Cluster 18 (K). Each dot represents a cell, with the color gradient from blue to red indicating increasing gene expression. (For interpretation of the references to color in this figure legend, the reader is referred to the web version of this article.)

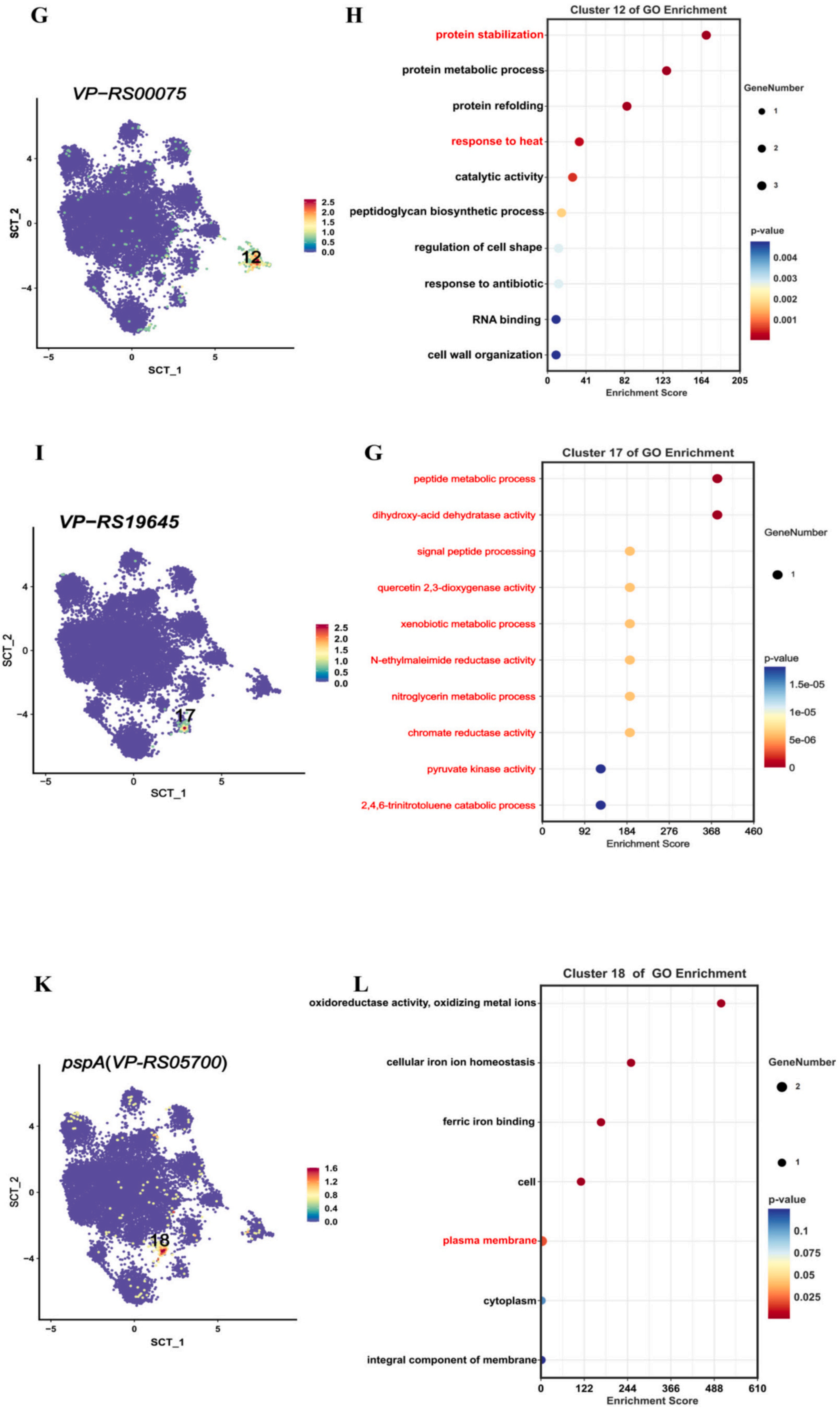

Fig. 4. (*continued*).

corresponds to *pspA*-expressing subpopulations (Cluster 18) executing membrane damage repair, a critical adaptation for surface colonization. Beyond these explicit linkages, latent survival modules like *gorA*-driven oxidative defense (Cluster 2) and NirD/YgiW/YdeI-mediated metabolic reprogramming (Cluster 17) represent novel tolerance nodes undetectable by bulk assays, collectively establishing an interdependent resistance network.

The time-dependent partial recovery of motility at 24 h suggests dynamic functional switching among subpopulations that may involve uncharacterized regulatory cascades or sequential activation of repair mechanisms. Current single-timepoint sampling likely missed transient transcriptional states critical to this recovery process. Similarly, the delayed growth inhibition observed at high ampicillin concentrations (500 μg/mL; Fig. 1F) implies temporal stratification of resistance mechanisms—where early efflux activity (Cluster 7) may transition to metabolic dormancy (Cluster 17) over extended exposure—but requires validation through time-resolved profiling. These observations highlight that functional specialization likely follows spatiotemporal hierarchies, with resistance adaptations accumulating progressively over time. The static nature of our snapshot analysis cannot resolve whether subpopulations arise stochastically or are induced sequentially under prolonged stress, nor can it capture potential spatial coordination within structured communities like biofilms, where *pspA*-expressing cells might localize to matrix interfaces to enhance community resilience.

Current technical limitations compound these gaps. scRNA-seq's reliance on random primers may miss non-polyadenylated transcripts (e.g., regulatory sRNAs), leading to undetected heterogeneity regulators. The absence of temporal and spatial resolution particularly obscures phenotypic-transcriptomic causality for dynamically evolving phenotypes and spatially organized functions. Furthermore, real-world co-exposure scenarios—such as concurrent heavy metal stress in aquaculture systems (Xiao et al., 2023)—may reshape subpopulation dynamics through cross-stress adaptation, a dimension not modeled in this study.

Future research should prioritize time-series scRNA-seq to map subpopulation succession during extended antibiotic exposure, spatial transcriptomics to resolve niche-specific roles in biofilms, and intestinal organoid models to assess the in vivo fitness of key subpopulations like *exsD*-expressing cells. In conclusion, the compartmentalization of resistance mechanisms across specialized subpopulations represents a sophisticated survival strategy where detoxification, structural maintenance, and metabolic flexibility are distributed across cellular task forces. As subinhibitory antibiotics permeate food chains, precisely disrupting functional coordination among these subpopulations—particularly efflux specialists (Cluster 7) and membrane protectors (Cluster 18)—will be essential for controlling multidrug-resistant vibrios in both clinical and environmental reservoirs.

GO-enriched bubble plots of marker genes in Cluster 2 (B), Cluster 7 (F), Cluster 12 (H), Cluster 17 (J), and Cluster 18 (L). The Y-axis represents gene function names, and the X-axis represents enrichment scores. Higher values indicate a greater proportion of differential genes associated with that function. VFDB database annotation results for Cluster 4 (D), where the X-axis represents the fold change of marker genes and the Y-axis represents the annotation results.

CRediT authorship contribution statement

Zhangxi Gong: Writing – original draft, Visualization, Validation, Methodology. **Yu Zhou:** Validation, Investigation, Formal analysis, Conceptualization. **Yongbing Ba:** Methodology, Investigation, Conceptualization. **Yao Yang:** Supervision, Software, Methodology. **Yingjie Pan:** Validation, Project administration, Data curation, Conceptualization. **Yong Zhao:** Methodology, Data curation, Conceptualization. **Haiquan Liu:** Writing – review & editing, Supervision, Funding acquisition, Data curation, Conceptualization.

Declaration of competing interest

This work was supported by the Shanghai Agriculture Applied Technology Development Program (Grant No. X2024-02-08-00-12-F00038).

Data availability

No data was used for the research described in the article.

References

Anggramukti, D.S., Ishii, E., Pratama, A., Al Kadi, M., Iida, T., Kodama, T., Matsuda, S., 2024. The read-through transcription-mediated autoactivation circuit for virulence regulator expression drives robust type III secretion system 2 expression in *Vibrio parahaemolyticus*. PLoS Pathog. 20 (3), e1012094. https://doi.org/10.1371/journal.ppat.1012094.

Arunima, A., Swain, S.K., Patra, S.D., Das, S., Mohakud, N.K., Misra, N., Suar, M., 2020. Role of OB-fold protein YdeI in stress response and virulence of *Salmonella enterica* serovar enteritidis. J. Bacteriol. 203 (1). https://doi.org/10.1128/jb.00237-20 e00237-e00220.

Belenky, P., Ye, Jonathan D., Porter, Caroline B.M., Cohen, Nadia R., Lobritz, Michael A., Ferrante, T., Jain, S., Korry, Benjamin J., Schwarz, Eric G., Walker, Graham C., Collins, James J., 2015. Bactericidal antibiotics induce toxic metabolic perturbations that lead to cellular damage. Cell Rep. 13 (5), 968–980. https://doi.org/10.1016/j.celrep.2015.09.059.

Bhowmick, A., Bhakta, K., Roy, M., Gupta, S., Das, J., Samanta, S., Patranabis, S., Ghosh, A., 2023. Heat shock response in *Sulfolobus acidocaldarius* and first implications for cross-stress adaptation. Res. Microbiol. 174 (8), 104106. https://doi.org/10.1016/j.resmic.2023.104106.

Brutinel, E.D., Vakulskas, C.A., Yahr, T.L., 2010. ExsD inhibits expression of the *Pseudomonas aeruginosa* type III secretion system by disrupting ExsA self-association and DNA binding activity. J. Bacteriol. 192 (6), 1479–1486. https://doi.org/10.1128/jb.01457-09.

Chen, J., Zhang, R., Qi, X., Zhou, B., Wang, J., Chen, Y., Zhang, H., 2017. Epidemiology of foodborne disease outbreaks caused by *Vibrio parahaemolyticus* during 2010–2014 in Zhejiang Province, China. Food Control 77, 110–115. https://doi.org/10.1016/j.foodcont.2017.02.004.

Chiou, J., Li, R., Chen, S., 2015. CARB-17 family of β-lactamases mediates intrinsic resistance to penicillins in *Vibrio parahaemolyticus*. Antimicrob. Agents Chemother. 59 (6), 3593–3595. https://doi.org/10.1128/aac.00047-15.

Cui, X., Sherman Wen, H.M., Kinoshita, Y., Koishi, S., Isowaki, C., Ou, L., Masuda, Y., Honjoh, K.I., Miyamoto, T., 2018. Role of phage shock protein in recovery of heat-injured *Salmonella*. Biocontrol Sci. 23 (1), 17–25. https://doi.org/10.4265/bio.23.17.

Fang, G.-Y., Liu, X.-Q., Mu, X.-J., Huang, B.-W., Jiang, Y.-J., 2023. Distinct increase in antimicrobial resistance genes among Vibrio parahaemolyticus in recent decades worldwide. Chemosphere 340, 139905. https://doi.org/10.1016/j.chemosphere.2023.139905.

Ghezzi, P., 2005. Regulation of protein function by glutathionylation. Free Radic. Res. 39 (6), 573–580. https://doi.org/10.1080/10715760500072172.

Guo, Z., Tang, X., Wang, W., Luo, Z., Zeng, Y., Zhou, N., Yu, Z., Wang, D., Song, B., Zhou, C., Xiong, W., 2025. The photo-based treatment technology simultaneously removes resistant bacteria and resistant genes from wastewater. J. Environ. Sci. 148, 243–262. https://doi.org/10.1016/j.jes.2024.01.005.

He, D., Yu, Q., Zeng, X., Feng, J., Yang, R., Wan, H., Zhong, Y., Yang, Y., Zhao, R., Lu, J., Zhang, J., 2023. Single-cell RNA sequencing and transcriptome analysis revealed the immune microenvironment and gene markers of acute respiratory distress syndrome. J. Inflamm. Res. 16, 3205–3217. https://doi.org/10.2147/jir.S419576.

Hedlund, E., Deng, Q., 2018. Single-cell RNA sequencing: technical advancements and biological applications. Mol. Aspects Med. 59, 36–46. https://doi.org/10.1016/j.mam.2017.07.003.

Herath, H.M.L.P.B., Wickramasinghe, P.D.S.U., Bathige, S.D.N.K., Jayasooriya, R.G.P.T., Kim, G.-Y., Park, M.A., Kim, C., Lee, J., 2017. Molecular identification and functional delineation of a glutathione reductase homolog from disk abalone (*Haliotis discus discus*): insights as a potent player in host antioxidant defense. Fish Shellfish Immunol. 60, 355–367. https://doi.org/10.1016/j.fsi.2016.12.002.

Huan, L.I.U., Ting, X.I.E., Mei-shan, H.E., Nan, D., Qing-ping, Z., 2018. Isolation, identification and antibiotic resistance analysis of *Vibrio parahaemolyticus* in seafood from Guangzhou. Food Ferment. Ind. 44 (11), 28–34. https://doi.org/10.13995/j.cnki.11-1802/ts.017408.

Ji, M., Barnwell, C.V., Grunden, A.M., 2015. Characterization of recombinant glutathione reductase from the psychrophilic Antarctic bacterium *Colwellia psychrerythraea*. Extremophiles 19 (4), 863–874. https://doi.org/10.1007/s00792-015-0762-1.

Jiang, Y., Yao, L., Li, F., Tan, Z., Zhai, Y., Wang, L., 2014. Characterization of antimicrobial resistance of *Vibrio parahaemolyticus* from cultured sea cucumbers (*Apostichopus japonicas*). Lett. Appl. Microbiol. 59 (2), 147–154. https://doi.org/10.1111/lam.12258.

Jiang, Y., Wang, P., Qu, M., Wang, T., Li, F., Wang, L., Yao, L., 2023. Effects of luxS gene on growth characteristics, biofilm formation, and antimicrobial resistance of multiantimicrobial-resistant Vibrio parahaemolyticus Vp2015094 isolated from shellfish. J. Appl. Microbiol. 134 (8). https://doi.org/10.1093/jambio/lxad172.

Junglas, B., Huber, S.T., Heidler, T., Schlösser, L., Mann, D., Hennig, R., Clarke, M., Hellmann, N., Schneider, D., Sachse, C., 2021. PspA adopts an ESCRT-III-like fold and remodels bacterial membranes. Cell 184 (14), 3674–3688 e3618. https://doi.org/10.1016/j.cell.2021.05.042.

Kuroda, T., Tsuchiya, T., 2009. Multidrug efflux transporters in the MATE family. Biochim. Biophys. Acta 1794 (5), 763–768. https://doi.org/10.1016/j.bbapap.2008.11.012.

Lee, J., Hiibel, S.R., Reardon, K.F., Wood, T.K., 2010. Identification of stress-related proteins in *Escherichia coli* using the pollutant *cis*-dichloroethylene. J. Appl. Microbiol. 108 (6), 2088–2102. https://doi.org/10.1111/j.1365-2672.2009.04611.x.

Léger, L., Byrne, D., Guiraud, P., Germain, E., Maisonneuve, E., 2021. NirD curtails the stringent response by inhibiting RelA activity in *Escherichia coli*. Elife 10, e64092. https://doi.org/10.7554/eLife.64092.

Lemée, P., Charron, R., Bridier, A., 2025. Genomic pipeline for analysis of mutational events in bacteria. Methods Mol. Biol. 2852, 211–222. https://doi.org/10.1007/978-1-0716-4100-2_15.

Li, H., Tang, R., Lou, Y., Cui, Z., Chen, W., Hong, Q., Zhang, Z., Malakar, P.K., Pan, Y., Zhao, Y., 2017. A comprehensive epidemiological research for clinical *Vibrio parahaemolyticus* in Shanghai. Front. Microbiol. 8, 1043. https://doi.org/10.3389/fmicb.2017.01043.

Li, N., Yongbing, B., Fengjia, B., Haiquan, L., Yingjie, P., Yong, Z., 2019. Comparison of antimicrobial resistance of vibrio parahaemolyticus isolated from different sources. J. Food Sci. Biotechnol. 38 (12), 9–16. https://kns.cnki.net/kcms2/article/abstract?v=_uHp55J8LtDYne66O5zlKP10ylcaJYVCQPXNIwhMYGH4AJZY-ZHC1oHLzELdsJrK9HrBMqzd1rvQjSvPiAzpRga80IGDEWn9nbQybKzywBiQ70VKWCzkpPU310sxCRQ1_lxzzj0sp3-wIG9MTW7og0-XyUrdRWJND0cr-he330u3Vp8v97Akjite7fdGvJxrgpRLjJ-jPhg=&uniplatform=NZKPT&language=CHS.

Lu, M., 2016. Structures of multidrug and toxic compound extrusion transporters and their mechanistic implications. Channels (Austin) 10 (2), 88–100. https://doi.org/10.1080/19336950.2015.1106654.

Ma, P., Amemiya, H.M., He, L.L., Gandhi, S.J., Nicol, R., Bhattacharyya, R.P., Smillie, C. S., Hung, D.T., 2023. Bacterial droplet-based single-cell RNA-seq reveals antibiotic-associated heterogeneous cellular states. Cell 186 (4), 877–891 e814. https://doi.org/10.1016/j.cell.2023.01.002.

Munita Jose, M., Arias Cesar, A., 2016. Mechanisms of antibiotic resistance. Microbiol. Spectr. 4 (2). https://doi.org/10.1128/microbiolspec.vmbf-0016-2015.

Plaza, N., Pérez-Reytor, D., Corsini, G., García, K., Urrutia, Í.M., 2024. Contribution of the type III secretion system (T3SS2) of Vibrio parahaemolyticus in mitochondrial stress in human intestinal cells. Microorganisms 12 (4), 813. https://www.mdpi.com/2076-2607/12/4/813.

Pranjal, Ghosh, S., Habeeb Rahman, A.P., Chakrabortty, S., Banerjee, S., Kumar, R., Mishra, A., Jeon, B.-H., Stålsby Lundborg, C., Tripathy, S.K., 2023. Homogenous Sono-Fenton reaction can trigger long term bactericidal effect against *Acinetobacter baumannii* due to residual stress induced by reactive oxygen species. Chem. Eng. J. 464, 142556. https://doi.org/10.1016/j.cej.2023.142556.

Qi, Y., Liu, D., Yu, H., Zhang, G., Fan, M., 2020. Identification and characterization of the small heat shock protein Hsp20 from *Oenococcus oeni* SD-2a. Curr. Microbiol. 77 (11), 3595–3602. https://doi.org/10.1007/s00284-020-02168-z.

Song, Z., Chen, L., Tang, S., Pan, Y., Xie, Q., Zhao, Y., Liu, H., 2025. Effects of low-salt stress on biological characteristics and transcriptomic profiles of *Vibrio parahaemolyticus*. Int. J. Food Microbiol. 430, 111047. https://doi.org/10.1016/j.ijfoodmicro.2024.111047.

Standar, K., Mehner, D., Osadnik, H., Berthelmann, F., Hause, G., Lünsdorf, H., Brüser, T., 2008. PspA can form large scaffolds in *Escherichia coli*. FEBS Lett. 582 (25–26), 3585–3589. https://doi.org/10.1016/j.febslet.2008.09.002.

Su, Y.-C., Liu, C., 2007. *Vibrio parahaemolyticus*: a concern of seafood safety. Food Microbiol. 24 (6), 549–558. https://doi.org/10.1016/j.fm.2007.01.005.

Tan, X., Qiao, J., Wang, J., Li, H., Wang, X., 2022. Characterization of ampicillin-resistant genes in *Vibrio parahaemolyticus*. Microb. Pathog. 168, 105573. https://doi.org/10.1016/j.micpath.2022.105573.

Tanabe, T., Tsukamoto, M., Shioda, M., Nagaoka, K., Funahashi, T., 2024. Expression regulation of type III secretion system 2 in *Vibrio parahaemolyticus* by catabolite activator protein. FEMS Microbiol. Lett. 371, fnae054. https://doi.org/10.1093/femsle/fnae054.

Upadhyay, V., Fu, Y.-X., 2013. Lymphotoxin signalling in immune homeostasis and the control of microorganisms. Nat. Rev. Immunol. 13 (4), 270–279. https://doi.org/10.1038/nri3406.

Urbanowski, M.L., Lykken, G.L., Yahr, T.L., 2005. A secreted regulatory protein couples transcription to the secretory activity of the Pseudomonas aeruginosa type III secretion system. Proc. Natl. Acad. Sci. U. S. A. 102 (28), 9930–9935. https://doi.org/10.1073/pnas.0504405102.

Velazquez-Roman, J., León-Sicairos, N., Hernandez-Diaz, L.D., Canizalez-Roman, A., 2014. Pandemic *Vibrio parahaemolyticus* O3:K6 on the American continent. Front. Cell. Infect. Microbiol. 3, 110. https://doi.org/10.3389/fcimb.2013.00110.

Vrancken, K., Van Mellaert, L., Anné, J., 2008. Characterization of the *Streptomyces lividans* PspA response. J. Bacteriol. 190 (10), 3475–3481. https://doi.org/10.1128/jb.01966-07.

Wang, J., Fu, D., Tian, Y., Lv, M., Xu, J., Yu, T., Lu, L., Pang, X., Li, X., 2025. Single-cell transcriptome sequencing (scRNA-seq) reveals dynamic gene expression trajectories regulating vascular cell senescence in *Hylocereus undatus*. Gene 966, 149718. https://doi.org/10.1016/j.gene.2025.149718.

Xiao, C., Qiao, Y., Yang, G., Feng, L., 2023. Antibiotics resistance evolution of isolated *Vibrio parahaemolyticus* from mariculture under the continuous culture of sub-inhibitory concentrations of Ulva fasciata hydroponic solution. Sci. Total Environ. 859, 160124. https://doi.org/10.1016/j.scitotenv.2022.160124.

Xiaofeng, W., Chunhong, Z., Yunyan, C., Youxian, Z., 2023. Drug resistance characteristics and molecular typing of Vibrio parahaemolyticus isolated fromfood contamination risk monitoring in Quanzhou City from 2017 to 2021. Chin. J. Food Hygiene 35 (09), 1328–1332. https://doi.org/10.13590/j.cjfh.2023.09.012.

Xin, Y., Peng, S., Wei, S., Lei, Y., Zhang, S., Hu, Y., Lv, Y., 2023. Antimicrobial and biofilm inhibition effects of p-anisaldehyde against *Vibrio parahaemolyticus*. Food Control 154, 110021. https://doi.org/10.1016/j.foodcont.2023.110021.

Xu, Z., Wang, Y., Sheng, K., Rosenthal, R., Liu, N., Hua, X., Zhang, T., Chen, J., Song, M., Lv, Y., Zhang, S., Huang, Y., Wang, Z., Cao, T., Shen, Y., Jiang, Y., Yu, Y., Chen, Y., Guo, G., Yin, P., Weitz, D.A., Wang, Y., 2023. Droplet-based high-throughput single microbe RNA sequencing by smRandom-seq. Nat. Commun. 14 (1), 5130. https://doi.org/10.1038/s41467-023-40137-9.

Yang, Y., Li, J., Yin, Y., Guo, D., Jin, T., Guan, N., Shi, Y., Xu, Y., Liang, S., Xia, X., Shi, C., 2019. Antibiofilm activity of coenzyme Q0 against *Salmonella* typhimurium and its effect on adhesion-invasion and survival-replication. Appl. Microbiol. Biotechnol. 103 (20), 8545–8557. https://doi.org/10.1007/s00253-019-10095-8.

Yu, Q., Niu, M., Yu, M., Liu, Y., Wang, D., Shi, X., 2016. Prevalence and antimicrobial susceptibility of Vibrio parahaemolyticus isolated from retail shellfish in Shanghai. Food Control 60, 263–268.

Yu, M., Jiang, C., Meng, Y., Wang, F., Qian, J., Fei, F., Yin, Z., Zhao, W., Zhao, Y., Liu, H., 2023. Effect of low temperature on the resistance of *Listeria monocytogenes* and *Escherichia coli* O157:H7 to acid electrolyzed water. Food Res. Int. 168, 112776. https://doi.org/10.1016/j.foodres.2023.112776.

Yusof, N.A., Hashim, N.H., Beddoe, T., Mahadi, N.M., Illias, R.M., Bakar, F.D., Murad, A. M., 2016. Thermotolerance and molecular chaperone function of an SGT1-like protein from the psychrophilic *yeast, Glaciozyma antarctica*. Cell Stress Chaperones 21 (4), 707–715. https://doi.org/10.1007/s12192-016-0696-2.

Zeng, Q., Lai, P., Huang, M., Peng, X., Huang, J., Chen, Q., Chen, Y., Wang, H., 2024. MAM7 from *Vibrio parahaemolyticus*: expression, purification and effects on RAW264.7 cells. Protein Expr. Purif. 224, 106579. https://doi.org/10.1016/j.pep.2024.106579.

Zhang, L., Orth, K., 2013. Virulence determinants for *Vibrio parahaemolyticus* infection. Curr. Opin. Microbiol. 16 (1), 70–77. https://doi.org/10.1016/j.mib.2013.02.002.

Zhang, Y., Liu, H., Gu, D., Lu, X., Zhou, X., Xia, X., 2020. Transcriptomic analysis of PhoR reveals its role in regulation of swarming motility and T3SS expression in *Vibrio parahaemolyticus*. Microbiol. Res. 235, 126448. https://doi.org/10.1016/j.micres.2020.126448.

Zhang, P., Ji, L., Yan, W., Chen, L., Zhu, X., Lu, Z., Dong, F., 2024. Whole-genome sequencing and transcriptome-characterized mechanism of streptomycin resistance in *Vibrio parahaemolyticus* O10: K4. Infect. Genet. Evol. 117, 105540. https://doi.org/10.1016/j.meegid.2023.105540.

Zheng, J., Shi, B., Sun, J., Pan, Y., Ding, Y., Shi, X., Zhang, J., Zhang, H., He, J., Zhang, K., Shi, J., Bai, Y., Zhao, W., Wang, J., 2025. Global phylogeography and genomic characterization of *Vibrio parahaemolyticus* infections in Jilin province, China (2016–2022). Int. J. Food Microbiol. 428, 110993. https://doi.org/10.1016/j.ijfoodmicro.2024.110993.

Zhou, X., Konkel, M.E., Call, D.R., 2010. Regulation of type III secretion system 1 gene expression in *Vibrio parahaemolyticus* is dependent on interactions between ExsA, ExsC, and ExsD. Virulence 1 (4), 260–272. https://doi.org/10.4161/viru.1.4.12318.

Zhu, W., Chen, S., Cao, Y., Wang, A., Guo, J., Jia, J., Wang, H., Xia, X., 2025. Antibiofilm activity of rosmarinic acid against *Vibrio parahaemolyticus* in *vitro* and its efficacy in food systems. Food Biosci. 68, 106750. https://doi.org/10.1016/j.fbio.2025.106750.